# Defects in mitophagy promote redox-driven metabolic syndrome in the absence of TP53INP1

Marion Seillier, Laurent Pouyet, Prudence N'guessan, Marie Nollet, Florence Capo, Fabienne Guillaumond, Laure Peyta, Jean-François Dumas, Annie Varrault, Gyslaine Bertrand, et al.

# Defects in mitophagy promote redox-driven metabolic syndrome in the absence of TP53INP1

Marion Seillier[1,2,3,4], Laurent Pouyet[1,2,3,4], Prudence N'Guessan[1,2,3,4], Marie Nollet[1,2,3,4], Florence Capo[1,2,3,4], Fabienne Guillaumond[1,2,3,4], Laure Peyta[5], Jean-François Dumas[5], Annie Varrault[6], Gyslaine Bertrand[6], Stéphanie Bonnafous[7,8,9], Albert Tran[7,8,9], Gargi Meur[10], Piero Marchetti[11], Magalie A Ravier[6], Stéphane Dalle[6], Philippe Gual[7,8,9], Dany Muller[6], Guy A Rutter[10], Stéphane Servais[5], Juan L Iovanna[1,2,3,4] & Alice Carrier[1,2,3,4,*]

## Abstract

The metabolic syndrome covers metabolic abnormalities including obesity and type 2 diabetes (T2D). T2D is characterized by insulin resistance resulting from both environmental and genetic factors. A genome-wide association study (GWAS) published in 2010 identified *TP53INP1* as a new T2D susceptibility locus, but a pathological mechanism was not identified. In this work, we show that mice lacking TP53INP1 are prone to redox-driven obesity and insulin resistance. Furthermore, we demonstrate that the reactive oxygen species increase in TP53INP1-deficient cells results from accumulation of defective mitochondria associated with impaired PINK/PARKIN mitophagy. This chronic oxidative stress also favors accumulation of lipid droplets. Taken together, our data provide evidence that the GWAS-identified *TP53INP1* gene prevents metabolic syndrome, through a mechanism involving prevention of oxidative stress by mitochondrial homeostasis regulation. In conclusion, this study highlights TP53INP1 as a molecular regulator of redox-driven metabolic syndrome and provides a new preclinical mouse model for metabolic syndrome clinical research.

## Introduction

Metabolic syndrome (MS) describes a cluster of metabolic abnormalities including obesity, insulin resistance, hypertension and dyslipidemia (Pothiwala *et al*, 2009). The prevalence of MS has been increasing exponentially in the last few decades, paralleling the obesity epidemic. Obesity, which is defined as a body mass index $\geq 30 \text{ kg/m}^2$, results from accumulation of white adipose tissue. It depends on both genetic and environmental factors, in particular lifestyles featuring increased nutrient caloric intake but decreased calorie consumption. Diet may have a major role in the pathogenesis and prevalence of obesity (Calder *et al*, 2011), but other causes have to be considered, such as gut microbiota which affect host nutritional metabolism (Musso *et al*, 2010; Greiner & Backhed, 2011), and lack of physical exercise (Calder *et al*, 2011). Excess body weight is a major public health concern since it is associated with increased risk of cardiovascular disease, type 2 diabetes (T2D), Alzheimer's disease and cancer (van Kruijsdijk *et al*, 2009; Siegel & Zhu, 2009; Forte *et al*, 2012; Leboucher *et al*, 2013).

One major link between obesity and associated diseases is the chronic low-grade inflammatory state observed in obese patients (Calder *et al*, 2011; Gregor & Hotamisligil, 2011). Inflammation is induced by excessive accumulation of lipids in adipose tissue leading to adipocyte stress and release of inflammatory cytokines and adipokines. The resulting recruitment of immune cells to key metabolic organs further contributes to chronic inflammation. Obesity-associated immune signals concern all types of immune cells that prompt inflammation, as well as adipocytes themselves (Chawla *et al*, 2011; Deng *et al*, 2013). Importantly, the

obesity-associated chronic low-grade inflammatory state impacts all organs in the body. Hence, obese patients are at increased risk of developing cancer in any localization even if pancreatic and liver cancers show the highest increase in risk (Siegel & Zhu, 2009).

Inflammation is associated with oxidative stress which is one obesity-related feature participating in the development of MS (Bondia-Pons *et al*, 2012; Khoo *et al*, 2012; Rolo *et al*, 2012; Crujeiras *et al*, 2013). Oxidative stress results from excess of reactive oxygen species (ROS) production overwhelming antioxidant defenses (Pouyet & Carrier, 2010). ROS are mainly produced as by-products of the mitochondrial electron transport chain involved in ATP production (oxidative phosphorylation). Excess fatty acids and glucose are known to be deleterious for mitochondrial function, thus increasing ROS production. ROS can oxidize cell macromolecules, leading to impaired cellular homeostasis and associated pathologies such as cancer (Gupta *et al*, 2012; Crujeiras *et al*, 2013).

In the recent years, we have provided evidence that tumor protein 53-induced nuclear protein 1 (TP53INP1) is a key stress protein with antioxidant-associated tumor suppressive function (Gironella *et al*, 2007; Gommeaux *et al*, 2007; Cano *et al*, 2009; N'Guessan *et al*, 2011; Seux *et al*, 2011). The *TP53INP1* gene (a transcriptional target of p53 and other transcription factors) is highly conserved between human and rodents and over-expressed during stress response including inflammation (Tomasini *et al*, 2001; Jiang *et al*, 2004). TP53INP1-deficient mice, which lack participation of TP53INP1 in stress resolution, are prone to stress-induced dysfunctions including cancer (Gironella *et al*, 2007; Gommeaux *et al*, 2007; Cano *et al*, 2009; N'Guessan *et al*, 2011). Moreover, these mutant mice show a chronic oxidative stress characterized by an increase in the cell ROS level as well as a decrease of antioxidant defenses (Gommeaux *et al*, 2007; Cano *et al*, 2009; N'Guessan *et al*, 2011). Restoration of TP53INP1 expression in TP53INP1-deficient cells rescues the phenotype by alleviating ROS burden (Cano *et al*, 2009).

We demonstrated that TP53INP1 impacts on p53 and p73 transcriptional activity by direct interaction and mediates the antioxidant activity of p53 (Tomasini *et al*, 2003, 2005; Cano *et al*, 2009). The tumor suppressor p53 is a fascinating protein endowed with multiple functions, including metabolic regulation, in common with two other members of this family: p63 and p73 (Maddocks & Vousden, 2011; Rufini *et al*, 2012; Su *et al*, 2012; Liang *et al*, 2013). We also provided evidence for a role of TP53INP1 in autophagy by direct interaction with mammalian Atg8 orthologs including LC3 (Seillier *et al*, 2012). Autophagy is a catabolic process involved in the cellular energetic balance and lipid homeostasis thus regulating obesity (Singh & Cuervo, 2011; Lavallard *et al*, 2012). Interestingly, a genome-wide association study (GWAS) published in 2010 identified *TP53INP1* as a new T2D susceptibility locus (Voight *et al*, 2010). Collectively, those observations led us to address the role of TP53INP1 in metabolic regulation. We used TP53INP1-deficient mice to assess *in vivo* the effect of a high-fat diet which favors obesity, insulin resistance and T2D, and we investigated the cellular metabolic defects induced by TP53INP1 deficiency. In this work, we provide the demonstration that TP53INP1 is a primary molecular link between oxidative stress and MS.

# Results

## Absence of TP53INP1 favors obesity in a redox-dependent manner *in vivo*

We initially observed that the body weight of 5-month-old TP53INP1-deficient (KO or −/−) mice was higher than WT (+/+) in both males and females (Supplementary Fig S1A) and that fat mass was more abundant in TP53INP1-deficient than in WT mice (Supplementary Fig S1B). We supplemented drinking water with the anti-oxidant *N*-acetylcysteine (NAC) which alleviates chronic oxidative stress associated with TP53INP1 deficiency through increase of intracellular glutathione level (Cano *et al*, 2009; N'Guessan *et al*, 2011). NAC supplementation completely abolished fat mass difference between TP53INP1-deficient and WT mice (Supplementary Fig S1A and B). We then fed 8-week-old mice with a high-fat diet (HFD, 60% fat) (control (CTRL) food is 10% fat) during 16 weeks. We observed a higher body weight gain in HFD-fed TP53INP1 KO than WT mice (Fig 1A and Supplementary Fig S2A), although food consumption did not differ between genotypes (Supplementary Fig S3). Epididymal and renal fat masses were higher in KO than in WT mice upon HFD (Fig 1B and Supplementary Fig S2A). HFD-induced liver weight increase was also higher in HFD-fed TP53INP1 KO mice than WT (Fig 1B and Supplementary Fig S2A). HFD-induced steatosis (accumulation of lipid droplets in hepatocytes), assessed by histological analysis, was greater in KO than in WT mice (Supplementary Fig S2B). Taken together, those data show that TP53INP1-deficient mice are prone to obesity and liver complications, suggesting a role of TP53INP1 in dampening fat storage. Interestingly, the gene encoding TP53INP1 was over-expressed in the liver of HFD-fed C57BL/6 mice (Supplementary Fig S2C). Furthermore, in human, morbidly obese patients with hepatic steatosis showed an increase in hepatic *TP53INP1* expression, and *TP53INP1* expression was correlated with the level of a marker of hepatocyte death (keratin 18), with the grade of steatosis and with the expression level of the stress marker NQO1 (Supplementary Fig S2D–H and Supplementary Table S2). This suggests that *TP53INP1* expression is induced as part of an obesity-associated stress response and that this protective function is lacking in TP53INP1-deficient mice, thus impairing fat homeostasis.

In order to evaluate the impact of chronic oxidative stress in obesity predisposition of TP53INP1 KO mice, we treated the mice with NAC at the starting of HFD. Whereas NAC treatment did not modify final weight gain in HFD-fed WT mice, it completely abolished all body weight, organ weight and hepatic steatosis differences between HFD-fed KO and WT mice, bringing the KO mice values to those of the WT (Fig 1 and Supplementary Fig S2B). These results illustrate that chronic oxidative stress affecting the TP53INP1-deficient mice predisposes them to increased weight gain and adiposity, further favoring obesity and hepatic steatosis when challenged with a lipid-rich diet.

## Insulin resistance establishment is elicited by chronic oxidative stress induced by TP53INP1 deficiency *in vivo*

As obesity is generally associated with insulin resistance (IR), we investigated the susceptibility of HFD-fed TP53INP1-deficient mice to develop IR, glucose intolerance and hyperinsulinemia. We
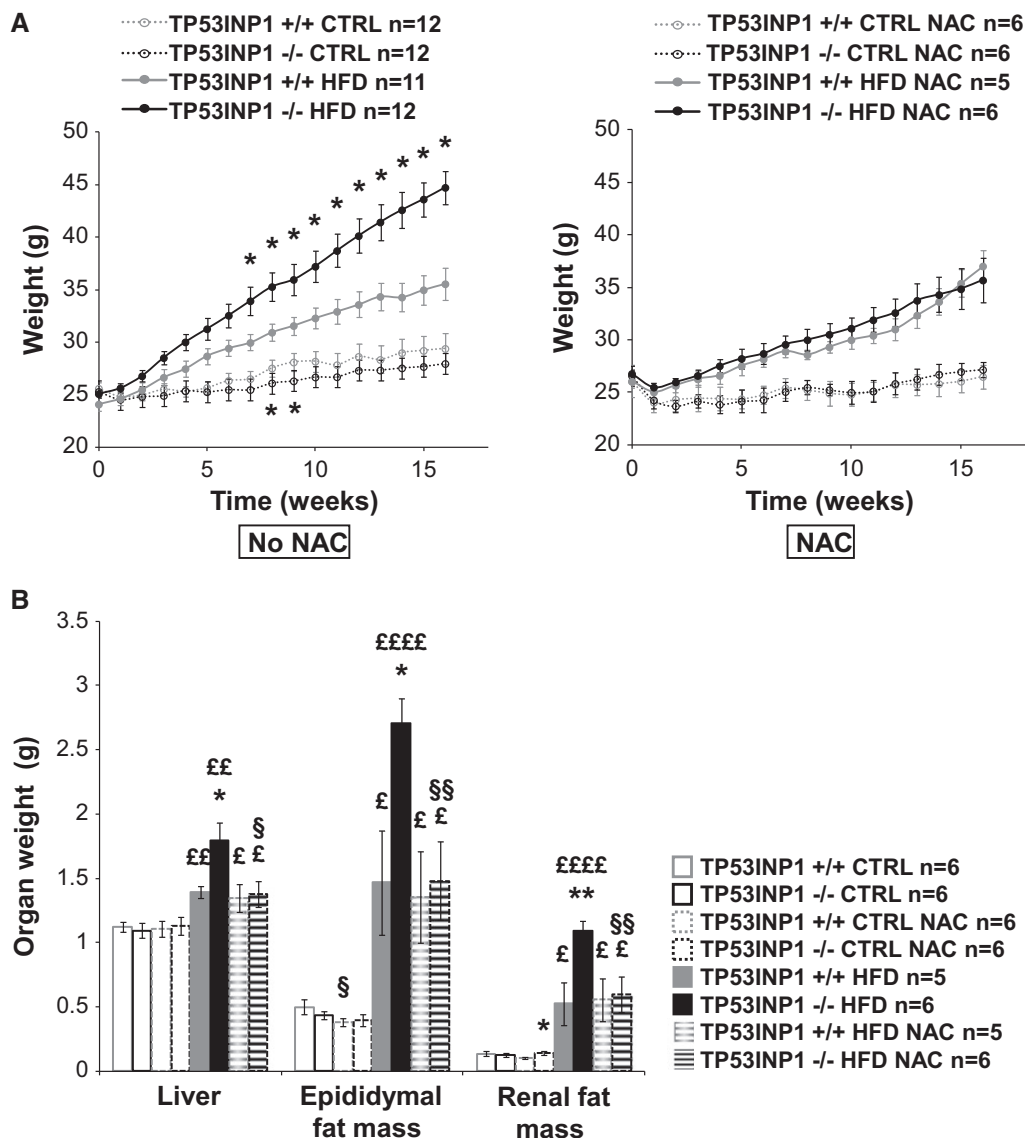
**Figure 1.  TP53INP1-deficient mice are highly susceptible to HFD-induced obesity owing to their chronic oxidative stress.**

TP53INP1-KO (−/−) and WT (+/+) male mice were subjected to a high-fat diet (HFD, 60% fat) or a control diet (CTRL) for 16 weeks. Mice drank tap water or tap water supplemented with NAC (10 mg/ml or 1%).

A   Curves show mice body weight recorded every week. CTRL: $P$ (−/− versus +/+; $t$ = 8w) = 0.047; $P$ (−/− versus +/+; $t$ = 9w) = 0.023. HFD: $P$ (−/− versus +/+; $t$ = 7w) = 0.039; $P$ (−/− versus +/+; $t$ = 8w) = 0.029; $P$ (−/− versus +/+; $t$ = 9w) = 0.021; $P$ (−/− versus +/+; $t$ = 10w) = 0.014; $P$ (−/− versus +/+; $t$ = 11w) = 0.0046; $P$ (−/− versus +/+; $t$ = 12w) = 0.0028; $P$ (−/− versus +/+; $t$ = 13w) = 0.0025; $P$ (−/− versus +/+; $t$ = 14w) = 0.00051; $P$ (−/− versus +/+; $t$ = 15w) = 0.00027; $P$ (−/− versus +/+; $t$ = 16w) = 0.00013.

B   At the end of protocol, mice were sacrificed; liver and epididymal and renal fat masses were taken and weighed. Histograms show organ weight. Liver: $P$ (−/− versus +/+; HFD) = 0.014; $P$ (HFD versus CTRL; +/+) = 0.00063; $P$ (HFD versus CTRL; −/−) = 0.0010; $P$ (HFD versus CTRL; +/+ NAC) = 0.034; $P$ (HFD versus CTRL; −/− NAC) = 0.027; $P$ (NAC versus no NAC; −/− HFD) = 0.014. Epididymal fat mass: $P$ (−/− versus +/+; HFD) = 0.011; $P$ (HFD versus CTRL; +/+) = 0.028; $P$ (HFD versus CTRL; −/−) = 0.000017; $P$ (HFD versus CTRL; +/+ NAC) = 0.019; $P$ (HFD versus CTRL; −/− NAC) = 0.0054; $P$ (NAC versus no NAC; +/+ CTRL) = 0.037; $P$ (NAC versus no NAC; −/− HFD) = 0.0025. Renal fat mass: $P$ (−/− versus +/+; HFD) = 0.0041; $P$ (HFD versus CTRL; +/+) = 0.028; $P$ (HFD versus CTRL; −/−) = 0.000013; $P$ (HFD versus CTRL; +/+ NAC) = 0.019; $P$ (HFD versus CTRL; −/− NAC) = 0.0078; $P$ (NAC versus no NAC; −/− HFD) = 0.0047.

Data information: Results are expressed as the mean ± SEM and are representative of two independent experiments. * −/− versus +/+; £ HFD versus CTRL; § NAC versus no NAC; 1 character: $P < 0.05$; 2 characters: $P < 0.005$; 4 characters: $P < 0.00005$.

monitored glycemia and insulinemia at the beginning and end of HFD protocol and determined the HOMA-IR index (Fig 2A and B, respectively, and Supplementary Table S1). We also performed glucose tolerance (GTT) and insulin tolerance (ITT) tests at the end

of HFD protocol (Fig 2C and D, respectively). In HFD-fed WT animals, glucose utilization (GTT, Fig 2C) and insulin sensitivity (ITT, Fig 2D) were both altered as expected. This was compensated by hyperinsulinemia (Fig 2B), while blood glucose remained

**Figure 2.**

unchanged (Fig 2A), indicating that WT mice under HFD have developed IR. Interestingly, TP53INP1 knockout mice fed a standard diet were also glucose intolerant and insulin resistant, but neither hyperglycemic nor hyperinsulinemic. Glucose intolerance and IR further developed when TP53INP1-deficient mice were fed a HFD, and hyperinsulinemia finally occurred in such experimental conditions with plasma insulin levels twice as high in HFD-fed TP53INP1-deficient as

in WT animals. As a consequence, the combined effects of HFD-induced obesity and the absence of TP53INP1 led to hyperglycemia (Fig 2A and C), suggesting that these mice had developed T2D. In contrast, NAC-treated HFD-fed TP53INP1-deficient mice showed similar metabolic profiles to HFD-fed WT animals (Fig 2A and B) indicative of chronic oxidative stress predisposing those mice to systemic IR, hyperinsulinemia, glucose intolerance and therefore T2D.

◄

**Figure 2. TP53INP1-deficient mice have moderate redox-related insulin resistance syndrome which is exacerbated by HFD protocol.**

Male TP53INP1 KO and WT mice were fed a high-fat diet (HFD, 60% fat) or a control diet (CTRL) during 16 weeks. Mice drank tap water or NAC-supplemented tap water (1%).

A, B  Histograms show blood glucose (A) or plasma insulin (B) levels of 6-h-fasted mice at the beginning (Week 0) and/or at the end of the protocol (Week 16). Fasting blood glucose week 16: $P$ (−/− versus +/+; HFD) = 0.0052; $P$ (CTRL versus HFD; −/−) = 0.000081; $P$ (NAC versus no NAC; −/− HFD) = 0.0019; $P$ (w16 versus w0; +/+ CTRL) = 0.012; $P$ (w16 versus w0; −/− CTRL) = 0.050; $P$ (w16 versus w0; −/− HFD) = 0.0023. Fasting plasma insulin: $P$ (−/− versus +/+; HFD) = 0.043; $P$ (CTRL versus HFD; +/+) = 0.028; $P$ (CTRL versus HFD; −/−) = 0.013; $P$ (CTRL versus HFD; +/+ NAC) = 0.011; $P$ (CTRL versus HFD; −/− NAC) = 0.0015; $P$ (NAC versus no NAC; −/− HFD) = 0.038.

C  Glucose tolerance test (GTT) was performed on 6-h-fasted mice during 120 min after injection of 1 g glucose/kg of body weight. Curves on the left show blood glucose level monitored after injection of glucose. Histograms on the right show area under curve (AUC). Fasting blood glucose: $P$ (−/− versus +/+; CTRL; $t$ = 0 min) = 0.045; $P$ (−/− versus +/+; CTRL; $t$ = 15 min) = 0.013; $P$ (−/− versus +/+; CTRL; $t$ = 30 min) = 0.016; $P$ (−/− versus +/+; CTRL; $t$ = 60 min) = 0.030; $P$ (−/− versus +/+; CTRL; $t$ = 90 min) = 0.017; $P$ (−/− versus +/+; HFD; $t$ = 60 min) = 0.041; $P$ (−/− versus +/+; HFD; $t$ = 90 min) = 0.043; $P$ (−/− versus +/+; HFD; $t$ = 120 min) = 0.034; $P$ (HFD versus CTRL; +/+; $t$ = 15 min) = 0.0076; $P$ (HFD versus CTRL; +/+; $t$ = 30 min) = 0.0067; $P$ (HFD versus CTRL; +/+; $t$ = 60 min) = 0.00058; $P$ (HFD versus CTRL; +/+; $t$ = 90 min) = 0.0010; $P$ (HFD versus CTRL; +/+; $t$ = 120 min) = 0.023; $P$ (HFD versus CTRL; −/−; $t$ = 60 min) = 0.032. AUC: $P$ (−/− versus +/+; CTRL) = 0.023; $P$ (−/− versus +/+; HFD) = 0.035; $P$ (HFD versus CTRL; +/+) = 0.042.

D  Insulin tolerance test (ITT) was performed on 6-h-fasted mice during 150 min after injection of 0.70 U insulin/kg of body weight. Curves on the left show blood glucose level monitored after injection of insulin. Histograms on the right show area above curve (AAC). Fasting blood glucose: $P$ (−/− versus +/+; CTRL; $t$ = 15 min = 0.012; $P$ (−/− versus +/+; CTRL; $t$ = 30 min) = 0.022; $P$ (−/− versus +/+; HFD; $t$ = 0 min) = 0.027; $P$ (−/− versus +/+; HFD; $t$ = 15 min) = 0.011; $P$ (−/− versus +/+; HFD; $t$ = 30 min) = 0.0037; $P$ (−/− versus +/+; HFD; $t$ = 60 min) = 0.0028; $P$ (−/− versus +/+; HFD; $t$ = 90 min) = 0.041; $P$ (−/− versus +/+; HFD; $t$ = 120 min) = 0.0032; $P$ (−/− versus +/+; HFD; $t$ = 150 min) = 0.0025; $P$ (HFD versus CTRL; +/+; $t$ = 15 min) = 0.0082; $P$ (HFD versus CTRL; +/+; $t$ = 30 min) = 0.033; $P$ (HFD versus CTRL; +/+; $t$ = 90 min) = 0.047; $P$ (HFD versus CTRL; +/+; $t$ = 150 min) = 0.028; $P$ (HFD versus CTRL; −/−; $t$ = 15 min) = 0.026; $P$ (HFD versus CTRL; −/−; $t$ = 30 min) = 0.0095; $P$ (HFD versus CTRL; −/−; $t$ = 60 min) = 0.0031; $P$ (HFD versus CTRL; −/−; $t$ = 90 min) = 0.033; $P$ (HFD versus CTRL; −/−; $t$ = 120 min) = 0.0068; $P$ (HFD versus CTRL; −/−; $t$ = 150 min) = 0.0082. AAC: $P$ (−/− versus +/+; HFD) = 0.030; $P$ (HFD versus CTRL; −/−) = 0.037.

Data information: Results are expressed as the mean ± SEM and are representative of two independent experiments. * TP53INP1 −/− versus TP53INP1 +/+; £ HFD versus CTRL; $ Week 16 versus Week 0; § NAC versus no NAC; 1 character: $P < 0.05$; 2 characters: $P < 0.005$; 4 characters: $P < 0.00005$.

TP53INP1 mRNA has been reported to be present in human islets of Langerhans (~30th centile) (Eizirik *et al*, 2012). Using immunofluorescence to examine mouse pancreatic sections and human isolated β-cells (Fig 3A and B), and quantitative PCR analysis of rodent cells and endocrine tissues (Fig 3C and D), we found that *TP53INP1* was expressed both by pancreatic exocrine cells and by the insulin-secreting β-cells which play a central role in the control of glucose homeostasis. Because TP53INP1-deficient mice were glucose intolerant, and since *TP53INP1* transcripts were significantly increased in islets isolated from HFD-fed mice (Fig 3E), we next hypothesized that defects in β-cell function or plasticity could occur in TP53INP1 knockout mice. However, neither functional modifications (glucose-induced insulin secretion, NADP(H) or cytosolic free calcium concentration, $[Ca^{2+}]_c$) nor changes in islet mass were detected in the absence of TP53INP1 (Supplementary Fig S4). These results suggest that HFD-fed TP53INP1 KO mice developed diabetes due to severe IR, which resulted from whole-body redox deregulation rather than specific endocrine pancreatic alterations. Nonetheless, the observed failure of β-cell mass or function to increase in response to elevated insulin demand suggests that TP53INP1 may also be required in β-cells to mount a compensatory response to IR.

**Mitochondrial number is increased in the absence of TP53INP1, promoting chronic oxidative stress**

As susceptibility to obesity and T2D in TP53INP1-deficient mice is redox-linked, we addressed the question of the cellular origin of chronic oxidative stress in these mice (Gommeaux *et al*, 2007; Cano *et al*, 2009; N'Guessan *et al*, 2011). Oxidative stress could be due to ROS over-production in mitochondria which are the main source of ROS since superoxide is a by-product of respiratory chain (Murphy, 2009). We stained WT and TP53INP1-deficient cells (immortalized MEFs, depicted as MEFi in this manuscript) with a mitochondrial superoxide stain (MitoSox) and observed a fourfold higher level of staining in deficient cells compared to WT by flow

cytometry analysis (Fig 4A). Co-staining with the MitoTracker™ marker also showed that the mitochondrial mass was threefold higher in TP53INP1 KO cells than in WT (Fig 4B). Normalization of MitoSox to MitoTracker staining (Fig 4C) suggests that the increased mitochondrial mass is not the sole cause of ROS increase. Transmission electron microscopy (TEM; Fig 4D and E) revealed a higher number of mitochondria in TP53INP1-deficient cells than in WT. This difference was not affected by $H_2O_2$ (oxidative stress) treatment, suggesting that increase in mitochondrial number is the cause and not the consequence of chronic oxidative stress in the absence of TP53INP1. Together, those data demonstrate an increase in both mitochondrial number and ROS-producing activity in the absence of TP53INP1.

**Increased mitochondrial number in the absence of TP53INP1 stems from impaired mitophagy of dysfunctional mitochondrial pool**

We previously provided evidence for impaired autophagy in TP53INP1-deficient cells (N'Guessan *et al*, 2011; Seillier *et al*, 2012). Therefore, we addressed the possibility that dysregulation of the mitochondrial compartment might stem from the impaired elimination of damaged mitochondria by mitophagy. Treatment of MEFi with the autophagy inhibitor 3-MA (which blocks autophagy at early stage) led to both increased MitoSox and MitoTracker staining in WT cells (Fig 4A–C). Remarkably, this increase was not observed in TP53INP1-deficient cells, suggesting that autophagic flow leading to mitophagy must be chronically impaired in these cells. To gain further insight into this issue, we quantified the number of mitophagic vacuoles in MEFi. Figure 4D and E clearly show the presence of autophagic vacuoles containing mitochondria (entire or almost degraded) in TP53INP1 KO cells, whereas very few of these structures were seen in WT counterparts. As no change in mitochondrial mass was observed after autophagy inhibition in TP53INP1-deficient cells, this accumulation of mitophagic structures suggests a blockade of late stages in the mitophagic process, for example, fusion of
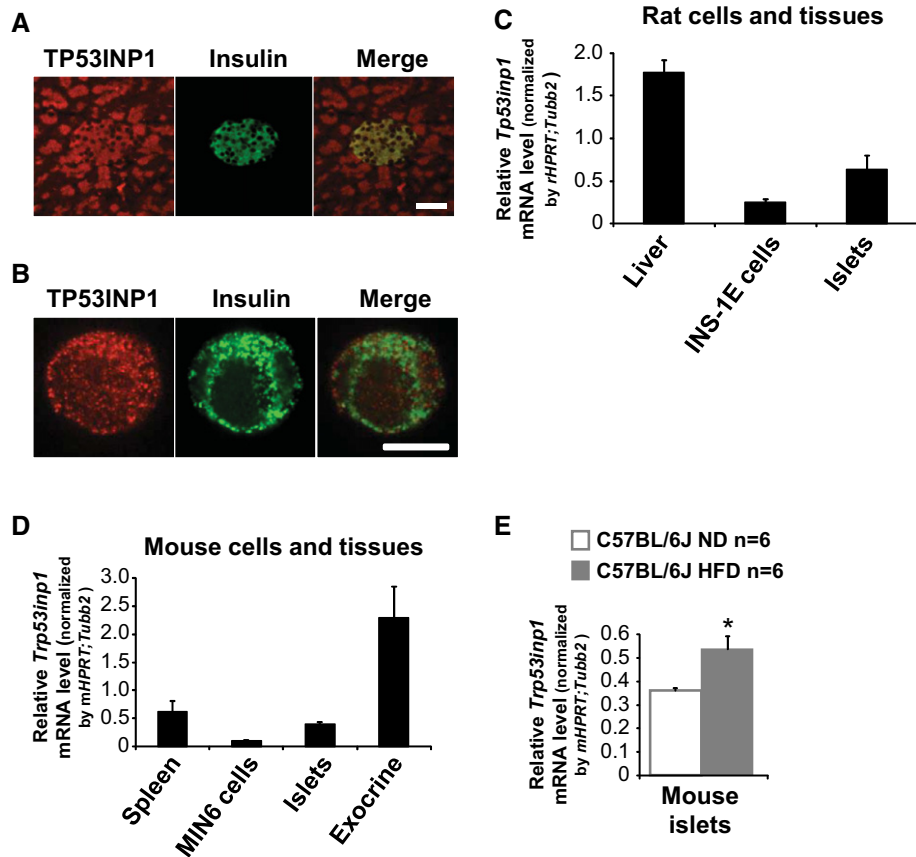
**Figure 3.  The gene encoding TP53INP1 is expressed in pancreatic endocrine cells.**

A, B    (A, B) Immunocytofluorescent staining of TP53INP1 (red) and insulin (green) in mouse pancreatic sections (A) and single human islet beta cell (B). Scale bars represent 50 μm (A) and 10 μm (B).

C–E    Quantitative PCR for *Tp53inp1* mRNA levels in tissues and cells from rat (C) and C57BL/6J mice fed with a normal diet (5% fat; ND) or an high-fat diet (45% fat; HFD) (D, E). Results are expressed as the mean ± SEM and are representative of two independent experiments. *n* = 2 for rat liver, islets and mouse spleen; *n* = 4 for INS-1E cells; *n* = 5 for mouse exocrine pancreas; *n* = 6 for Min6 cells and ND and HFD islets; *n* = 11 for mouse islets. *$P$ = 0.035 for HFD versus ND.

autophagosomes with lysosomes, rather than increased mitophagic flow. These results were unchanged after $H_2O_2$ treatment, suggesting that oxidative stress observed in the absence of TP53INP1 was the consequence and not the cause of a defect in mitochondria degradation. Higher number of mitophagic structures in TP53INP1 KO cells than in WT was also indicated by LC3/mitotracker co-labeling and quantification by confocal fluorescence microscopy (Supplementary Fig S5).

Western blot analysis performed on MEFi lysates (Fig 5A) showed higher levels of VDAC1, consistent with increased mitochondrial mass in TP53INP1 KO MEFi. By contrast, PINK1 and PARKIN levels were lowered in the absence of TP53INP1. As both PINK1 and PARKIN proteins are necessary for PINK/PARKIN-mediated mitophagy (following a loss of mitochondrial potential membrane in defective mitochondria) (Novak, 2012), this result is consistent with defective mitochondrial degradation by mitophagy. Neither oxidative stress nor antioxidant treatment ($H_2O_2$ and NAC treatment, respectively) impacted the lowered PINK1 and PARKIN levels in KO cells (Fig 5A). Surprisingly, BNIP3 and NIX protein levels were increased in TP53INP1 KO cells compared to WT, suggesting that hypoxia-induced mitophagy, which implicates BNIP3 and NIX

(Zhang & Ney, 2009), was not affected in TP53INP1-deficient cells. Lower PINK1 and PARKIN levels in the absence of TP53INP1 were also observed *in vivo* in mitochondria-enriched fractions from mouse liver (Fig 5C right). Nevertheless, the clear decrease in PINK1/PARKIN level and increase in VDAC level in TP53INP1 −/− cells (Fig 5A) were not totally recapitulated in the mice total liver lysates (Fig 5C left).

To gain insights into possible molecular partnerships between TP53INP1 and proteins involved in mitophagy, we performed immunoprecipitation assays. This provided further evidence for a direct interaction between each of the TP53INP1 isoforms (TP53INP1α or TP53INP1β) and both PINK1 and PARKIN, but not with BNIP3 or NIX (Fig 5B). Interestingly, Fig 5C shows detection of TP53INP1 in mitochondria-enriched fractions from WT liver, thus demonstrating a mitochondrial sub-cellular localization of TP53INP1, in addition to its known nucleo-cytoplasmic localization (Tomasini *et al*, 2001; Seillier *et al*, 2012). Moreover, restoration of TP53INP1 expression induced an increase in the level of both PINK1 and PARKIN in the mitochondrial fraction and confirmed localization of TP53INP1 to mitochondria (Supplementary Fig S6A). Finally, we observed a decreased level of PGC-1α (a regulator of
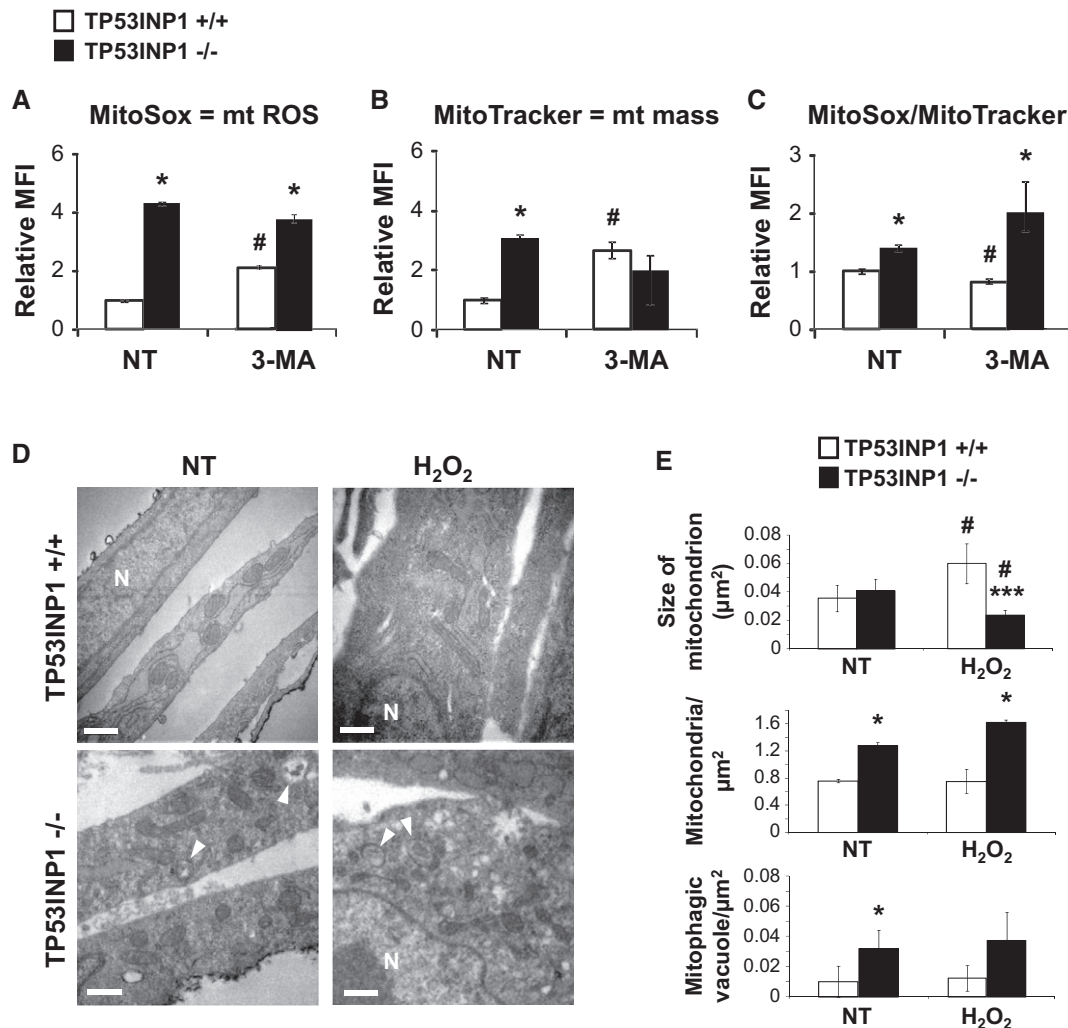
**Figure 4. Absence of TP53INP1 increases mitochondrial (mt) ROS level and mass due to increased mitochondria number.**

Immortalized MEFs (MEFi) deficient (−/−) or not (+/+) for TP53INP1 were left untreated (NT) or treated with 3-methyladenine (3-MA, 5 mM) during 4 h.

A  Histograms show mt ROS level measured by flow cytometry upon MitoSox staining. $P$ (−/− versus +/+; NT) = 0.019; $P$ (−/− versus +/+; 3-MA) = 0.025; $P$ (3-MA versus NT; +/+) = 0.031.

B  Histograms show mt mass evaluated by flow cytometry in KO or WT MEFi using MitoTracker staining. $P$ (−/− versus +/+; NT) = 0.012; $P$ (3-MA versus NT; +/+) = 0.036.

C  Histogram shows MitoSox fluorescence normalized with MitoTracker fluorescence. $P$ (−/− versus +/+; NT) = 0.041; $P$ (−/− versus +/+; 3-MA) = 0.030; $P$ (3-MA versus NT; +/+) = 0.045.

D  After 4 h recovering in normal media, $H_2O_2$ (1 h, 100 μM) or non-treated (NT) MEFi deficient (−/−) or not (+/+) for TP53INP1 were observed by transmission electron microscopy (TEM). N = nucleus; white arrow = mitophagic vacuoles. Scale bar represents 0.5 μm.

E  Mean size of mitochondrion (area), number of mitochondria and mitophagic vacuoles normalized by cytoplasmic surface area were quantified. Size: $P$ (−/− versus +/+; $H_2O_2$) = 0.000027; $P$ ($H_2O_2$ versus NT; +/+) = 0.0070; $P$ ($H_2O_2$ versus NT; −/−) = 0.013. Nb mito.: $P$ (−/− versus +/+; NT) = 0.035; $P$ (−/− versus +/+; $H_2O_2$) = 0.016. Nb vacuoles.: $P$ (−/− versus +/+; NT) = 0.047.

Data information: Results are expressed as the mean ± SEM and are representative of three independent experiments. In (A-C): *$P < 0.05$ for TP53INP1−/− versus TP53INP1 +/+; #$P < 0.05$ for 3-MA versus NT. In (E): * TP53INP1−/− versus TP53INP1 +/+; # $H_2O_2$ versus NT. 1 character: $P = 0.05$; 2 characters: $P < 0.01$; 3 characters: $P < 0.0005$.

mitochondrial biogenesis and function) in TP53INP1-deficient cells compared to WT (Fig 5A), suggesting that mitochondrial accumulation in the absence of TP53INP1 does not rely on increased mitochondrial biogenesis. (We cannot exclude the possibility that the absence of TP53INP1 rather negatively impacts on mitochondrial biogenesis.) Taken together, these data suggest that (i) at least large in part, accumulation of mitochondria in TP53INP1-deficient cells results from a mitophagic defect and (ii) that TP53INP1 is able to participate in the completion of PINK/PARKIN-dependent mitophagy by direct physical interaction with these proteins.

As part of mitochondrial ROS production was not related to an increase in mitochondrial mass (Fig 4C), we assessed whether mitochondrial over-production of ROS may be due to dysfunctional mitochondria. Mitochondrial oxygen consumption analysis showed
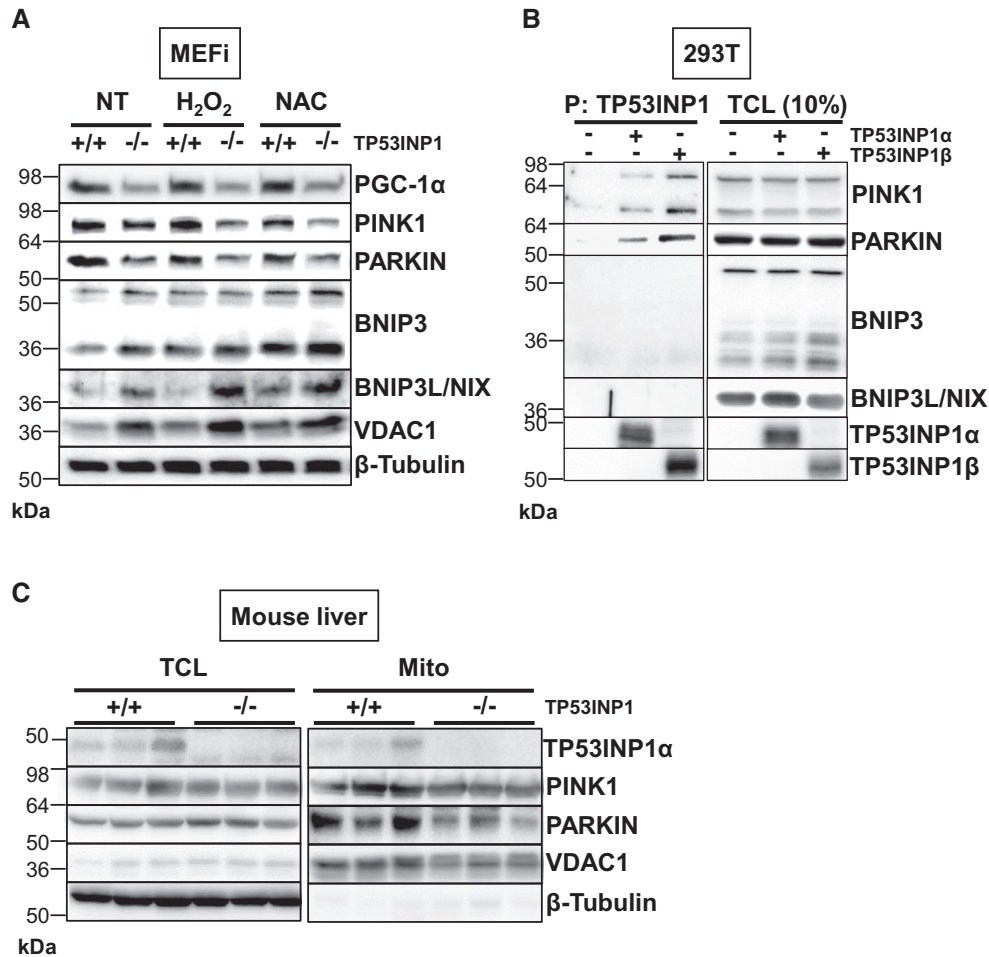
**Figure 5. TP53INP1 deficiency is linked with impaired PINK/PARKIN mitophagy.**

A   After 4 h recovering in normal media, TCLs from $H_2O_2$- (1 h, 100 μM), NAC- (24 h, 10 mM) or non-treated (NT) MEFi deficient (−/−) or not (+/+) for TP53INP1 were analyzed by immunoblotting for PGC-1α, PINK1, PARKIN, BNIP3, BNIP3L/NIX, VDAC1 and β-tubulin.

B   HEK293T cells were cotransfected with plasmids encoding TP53INP1α-NTAP or TP53INP1β-NTAP. TP53INP1α- or β-NTAP was precipitated with a streptavidin-containing resin (P), resolved by PAGE and Western blots developed with anti-TP53INP1 (TP53INP1 precipitation control), anti-PINK1, anti-PARKIN, anti-BNIP3 or anti-BNIP3L/NIX antibody. Western blot on TCL (on the right) served as a transfection control.

C   Three-month-old TP53INP1-deficient and WT male mice were sacrificed and their livers harvested. Mitochondrial lysates (Mito) were purified from total liver lysates (TCL), and both were analyzed by immunoblotting for TP53INP1, PINK1, PARKIN, VDAC1 and β-tubulin.

Data information: Results are representative of three independent experiments.
Source data are available online for this figure.

decreased oxygen flow in TP53INP1-deficient MEFi compared to WT, both in permeabilized and in intact cells, and whatever the substrate used (glucose versus lipid-related substrate) in the permeabilized cell setting (Fig 6A–C). Thus, the oxidative phosphorylation system of TP53INP1 KO MEFi is impaired compared to WT, probably resulting from specific mitochondrial alterations as similar observations were made in intact and permeabilized cells. Decreased oxygen consumption in the setting of lipid substrates (Fig 6C) is probably not related to decreased substrate availability since levels of CPT1A and CPT1B (two isoforms of CPT1, the key enzymes responsible for the mitochondrial uptake of long-chain fatty acids for beta-oxidation) did not differ between KO MEFi and WT cells (Fig 6E). Analysis of respiratory chain complexes showed decreased activity of complex IV (Fig 6D), without any change in

complex expression as quantified by Western blotting (L. Peyta, S. Servais, unpublished data). Finally, analysis of mitochondrial shape and size by transmission electron microscopy (TEM; Fig 4D and E) showed that upon $H_2O_2$ treatment, mitochondria became bigger (longer) in WT cells probably as a result of stress-induced mitochondrial fusion. By contrast, mitochondria occupied a smaller surface in $H_2O_2$-treated TP53INP1 KO cells, suggesting an impaired ability of TP53INP1-deficient mitochondria to cope with stress.

Collectively, our data show accumulation of defective mitochondria within TP53INP1-deficient MEFi associated with impaired mitophagy. The cumulative effect of increased mitochondrial number and their dysfunctional state is likely at the origin of ROS overproduction and chronic oxidative stress observed in the absence of TP53INP1.
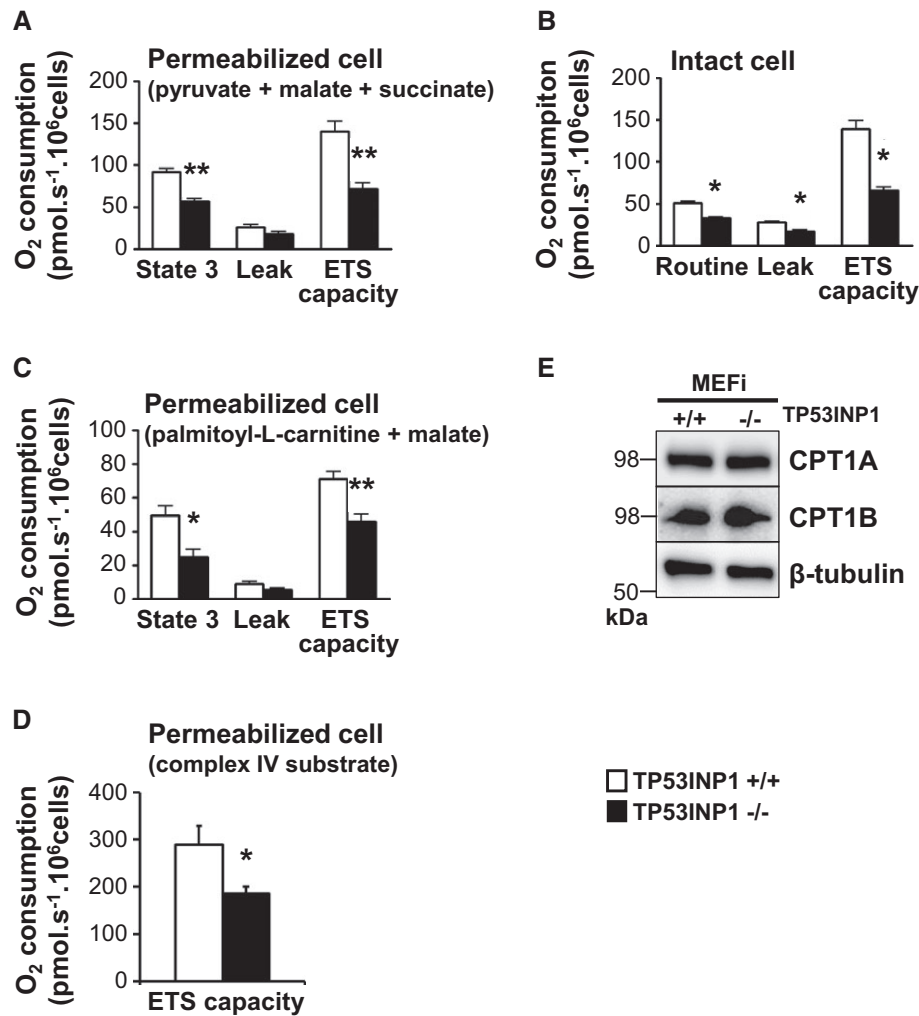
**Figure 6. TP53INP1-deficient MEFi contain a dysfunctional mitochondrial pool.**

A–D High-resolution respirometry was performed on permeabilized MEFi TP53INP1 deficient (−/−, black bars) or not (+/+, white bars) using glucose (A), lipid-related substrates (C) or complex IV substrate (D). High-resolution respirometry was also performed on intact MEFi (B). For different respiratory state details (routine, 3, leak, and ETS capacity), please refer to the Materials and Methods section. Results are expressed as the mean ± SEM and are representative of three independent experiments. In (A): $P$ (−/− versus +/+; State 3) = 0.0079; $P$ (−/− versus +/+; ETS) = 0.0079; $n$ = 5 in each group. In (B): $P$ (−/− versus +/+; routine) = 0.0159; $P$ (−/− versus +/+; leak) = 0.0159; $P$ (−/− versus +/+; ETS) = 0.0159; $n$ = 5 in each group. In (C): $P$ (−/− versus +/+; State 3) = 0.029; $P$ (−/− versus +/+; ETS) = 0.0079; $n$ = 5 in each group. In (D): $P$ (−/− versus +/+; ETS) = 0.0259; $n$ = 5 in each group. *TP53INP1−/− versus TP53INP1 +/+; 1 character: $P < 0.05$; 2 characters: $P < 0.01$.

E TCLs from MEFi were analyzed by immunoblotting for CPT1A, CPT1B and β-tubulin. Results are representative of three independent experiments.

Source data are available online for this figure.

## Accumulation of lipid droplets is linked with oxidative stress in TP53INP1-deficient cells

TEM analysis of MEFs revealed a huge number of lipid droplets (LD) in TP53INP1-deficient MEFi, whereas these were absent from control MEFs (Fig 7A). Staining of these LD using the fluorescent Bodipy compound (Fig 7B, left panel) confirmed that TP53INP1 KO MEFs contain far more LD than WT cells. To assess whether this feature could be linked to increased ROS production in deficient cells, we analyzed LD in $H_2O_2$-treated cells (Fig 7A and B). Upon oxidative stress, WT cells showed a striking increase in LD number which was not observed in TP53INP1 KO cells. Reciprocally, we treated cells with the antioxidant NAC (Fig 7B) and observed a reduction in LD number in both genotypes. Results obtained in primary MEFs corroborate those in MEFi (Supplementary Fig S7), showing that what we observed in MEFi is directly linked to the absence of TP53INP1 and not immortalization event(s). This study thus shows that oxidant treatment increases LD number in WT cells but, conversely, antioxidant treatment reduces LD number in TP53INP1 KO cells, both treatments abolishing differences existing between WT and KO cells. To gain molecular insight into these metabolic alterations, and based on a transcriptomic analysis of MEFi KO cells compared to WT (M. Seillier, A. Carrier, unpublished data), we showed by Western blotting an over-expression of PPARγ in KO cells, while expression of
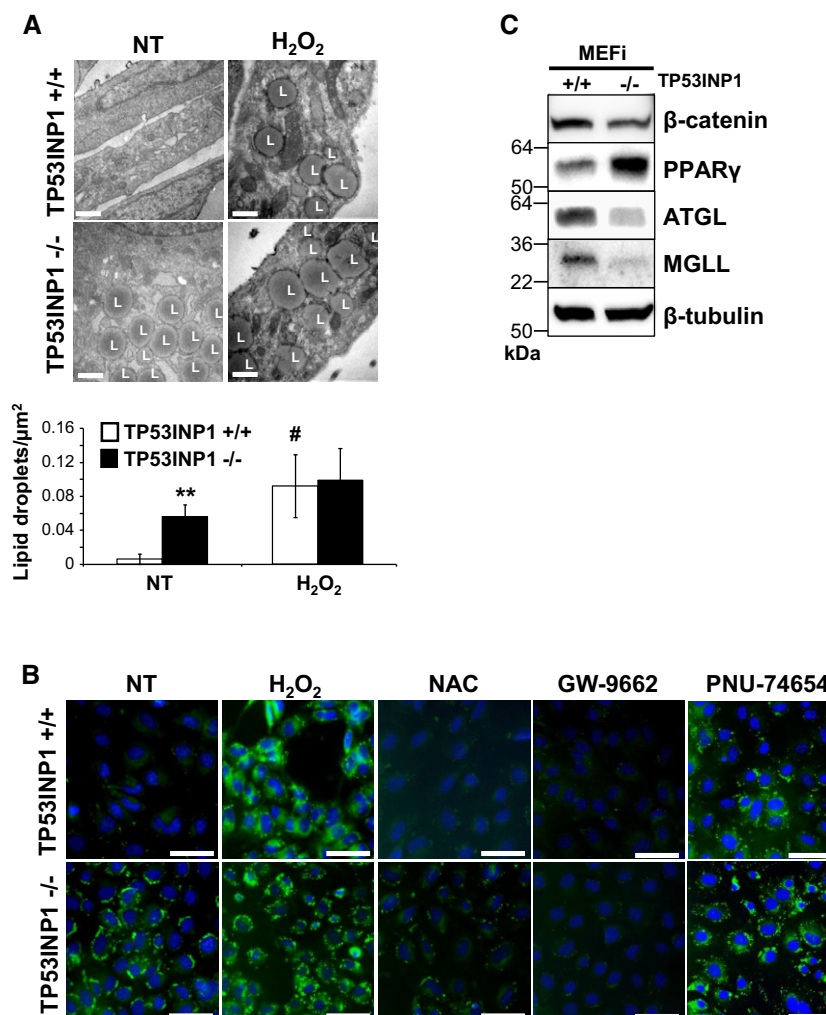
**Figure 7.  Oxidative stress observed in absence of TP53INP1 is at the origin of presence of lipid droplets (LD) in MEFi.**

MEFi deficient (−/−) or not (+/+) for TP53INP1 were seeded in media containing or not 10 mM NAC. Forty-eight hours later, MEFi were treated or not (NT) with 100 μM hydrogen peroxide ($H_2O_2$) during 1 h in serum free media. Cells were left to recover for 4 h in normal media containing or not NAC (10 mM), GW-9662 (PPARγ inhibitor, 10 μM) or PNU-74654 (Wnt/β-catenin pathway inhibitor, 50 μM) before being harvested. Cells were observed by TEM.

A   Number of LD normalized by cytoplasmic surface area is shown in both histograms at the bottom of the figure. Scale bar represents 0.5 μm. Results are expressed as the mean ± SEM and are representative of three independent experiments. *$P$ (−/− versus +/+; NT) = 0.00086; #$P$ ($H_2O_2$ versus NT; +/+) = 0.013.

B   Cells were also observed by fluorescence microscopy after Bodipy493/503 staining of LD (green) and DAPI staining of nucleus (blue). L = lipid droplets. Scale bar represents 100 μm. Results are representative of three independent experiments.

C   TCLs from MEFi were analyzed by immunoblotting for β-catenin, PPARγ, ATGL, MGLL and β-tubulin. Results are representative of three independent experiments.

Source data are available online for this figure.

β-catenin was decreased (Fig 7C). It is known that the Wnt/β-catenin pathway (canonical Wnt pathway) inhibits expression of the gene coding PPARγ, a positive regulator of adipo- and lipogenesis. Consistently, treatment with a PPARγ inhibitor (GW-9662) prevented LD accumulation, whereas treatment with a Wnt/β-catenin pathway inhibitor (PNU-74654) induced LD formation in both genotypes (Fig 7B), suggesting that regulation of PPARγ expression by canonical Wnt pathway is directly involved in LD accumulation in TP53INP1 KO cells. Finally, restoration of TP53INP1 expression led to decreased PPARγ expression (Supplementary Fig S6B) as well as decreased accumulation of LD (Supplementary Fig S6C). Western blotting analysis also showed decreased expression of lipases (ATGL and MGLL) in the absence of TP53INP1 (Fig 7C), in agreement with

increased LD content in MEFi KO cells. Taken together, those data provide molecular insights into redox-linked lipid metabolism defects in the absence of TP53INP1. We can conclude from these experiments that chronic oxidative stress observed in TP53INP1-deficient cells is at the origin of the accumulation of LD, which are likely involved in the *in vivo* increased fat depot and hepatic steatosis associated with HFD-induced obesity.

# Discussion

This work addresses the function of *TP53INP1* as a T2D susceptibility gene as proposed 5 years ago (Voight *et al*, 2010; Cauchi

*et al*, 2012) and provides both the demonstration and a mechanism for this function. We should note, however, that at present there is no evidence that the *TP53INP1* locus is associated with obesity in man. Nonetheless, in our mouse model, the absence of TP53INP1 favors increased body weight and fat mass, most spectacularly in an experimental setting of obesity induced by lipid-rich diet. Use of an antioxidant treatment, which alleviates the chronic oxidative stress affecting TP53INP1-deficient animals (N'Guessan *et al*, 2011), completely abolishes the predisposition to obesity, demonstrating that oxidative stress is the cause of exacerbated obesity in these animals. The present data thus provide the novel finding that oxidative stress may also be the cause of obesity and not only the well-known consequence of a chronic low-grade inflammatory state associated with obesity. By its action on redox status homeostasis, TP53INP1 is thus a new molecular actor of obesity prevention, and the current work thus adds to the knowledge of the molecular events involved in obesity predisposition.

We also observed that a lipid-rich diet reinforces the predisposition of TP53INP1-deficient mice to IR. Indeed, basal glycemia and insulinemia are high in obese (HFD-fed) TP53INP1-deficient mice, this feature being completely prevented by antioxidant treatment showing a key role of oxidative stress. Additionally, glycemia of obese TP53INP1-deficient mice is barely affected after insulin injection in the ITT experimental setting. Interestingly, glycemia of CTRL-fed TP53INP1-deficient mice follows the same curve as HFD-fed WT mice, suggesting that absence of TP53INP1 by itself favors IR usually related to obesity. Thus, emergence of IR in TP53INP1 mutant mice appears to result from chronic oxidative stress, without a requirement for increased adiposity. Adiposity may nonetheless strengthen the effects of the existing oxidative stress and IR, a novel observation of the current work. Importantly, our studies provide evidence, through the generation of animal model, of the molecular mechanisms through which the *TP53INP1* gene influences T2D predisposition in man (Voight *et al*, 2010). Intriguingly, our data suggest that antioxidants may be of use in individuals with T2D variants at the *TP53INP1* locus that affect diabetes risk.

We note that the variant at the *TP53INP1* locus on chromosome 8 (rs896854, lying in intron 1) associated with T2D in GWAS studies (Voight *et al*, 2010) appears to lead to impaired β-cell function (i.e. reduced insulin secretion), as measured by a decrease in HOMA-B (Voight *et al*, 2010) and unchanged insulin sensitivity. Moreover, dysglycemia necessarily involves a failure in pancreatic insulin secretion. The present data may suggest that, as well as being more insulin resistant, TP53INP1-deficient mice also possess β-cells which may be more susceptible to the effects of global lipid dysregulation. Interestingly, there are also decreases in miRNAs that regulate *TP53INP1* in human diabetic islets (Kameswaran *et al*, 2014), suggesting that over-expression of *TP53INP1* may occur in β-cells in diabetes. At present, it is unclear whether the risk variant at rs896854 affects the expression of *TP53INP1* (or that of other genes in this locus), in which tissues and in what direction. Future eQTL studies will be needed to answer this question.

Remarkably, our study provides a mechanism for TP53INP1 function in T2D. Increased predisposition of TP53INP1-deficient mice to adiposity is mirrored *in vitro* by a massive LD accumulation within TP53INP1-deficient cells, also dependent on chronic oxidative stress. At the molecular level, this LD accumulation in

TP53INP1 KO cells is directly correlated with decrease in lipases expression, but above all with decrease in β-catenin expression consistent with an increase of PPARγ expression. PPARγ is a major player in lipogenesis and LD formation whose expression is inhibited by the Wnt/β-catenin pathway (Moldes *et al*, 2003; Sahini & Borlak, 2014). Restoration of TP53INP1 expression decreases PPARγ expression as well as accumulation of LD in close link with dampening of oxidative stress (Cano *et al*, 2009). Taken together, these data provide molecular insights into redox-linked lipid metabolism defects in the absence of TP53INP1.

Regarding the origin of chronic oxidative stress associated with TP53INP1 deficiency, we provide data in favor of deregulated mitochondrial homeostasis in the absence of TP53INP1. We reveal that TP53INP1-deficient cells produce high levels of mitochondria-derived ROS, resulting from both respiratory chain defect and high number of mitochondria. Furthermore, we show that this latter is the consequence, at least in part, of impaired PINK/PARKIN mitophagy (Novak, 2012) in TP53INP1-deficient cells, consistent with our previous work reporting a role for TP53INP1 in autophagy (N'Guessan *et al*, 2011; Seillier *et al*, 2012). PINK/PARKIN mitophagy involves mitochondrial protein ubiquitination and p62 protein cargo. Interestingly, our laboratory previously provided evidence that TP53INP1 is able to compete with p62 for interaction with LC3 thanks to its better LIR affinity (Seillier *et al*, 2012). Thus, TP53INP1 could be directly involved in mitophagy by playing the role of a protein cargo directing mitochondria for degradation to autophagosomes. Alternatively, accumulation of mitophagic vacuoles in the absence of TP53INP1 could mean that TP53INP1 participates in the completion of PINK/PARKIN-dependent mitophagy. Data shown in the present work, that is, (i) a direct physical interaction of TP53INP1 with PINK1 and PARKIN, (ii) the influence of TP53INP1 expression on PINK1 and PARKIN levels in mitochondria (demonstrated both in loss- and gain-of-function cell models and in KO livers) and (iii) the subcellular localization of TP53INP1 in mitochondria, are in favor of the contribution of TP53INP1 in PINK/PARKIN-dependent mitophagy.

Finally, it is interesting to note that the TP53INP1 paralog TP53INP2 (also known as DOR for diabetes and obesity related) is also involved in MS through its implication in autophagy (Nowak *et al*, 2009; Mauvezin *et al*, 2010; Sala *et al*, 2014).

To conclude, this work provides a preclinical model of mice prone to MS. IR establishment in TP53INP1-deficient mice is favored by chronic oxidative stress, which drives LD accumulation. Furthermore, this work highlights the underlying mechanism by showing that chronic oxidative stress observed in the absence of TP53INP1 stems from impaired mitophagy of a dysfunctional mitochondrial pool (graphical abstract shown in Supplementary Fig S8). Therefore, TP53INP1 mutant mice constitute an original model in which to study the implication of oxidative stress and autophagy in the development of obesity and T2D, two crucial public health issues.

# Materials and Methods

### Mice

Generation of TP53INP1-deficient (*Trp53inp1*$^{-/-}$) mice backcrossed on the C57BL/6 parental genetic background and their genotyping

by PCR were described previously (Gommeaux *et al*, 2007; N'Guessan *et al*, 2011). TP53INP1 WT and KO mice originate from heterozygous (*Trp53inp1$^{+/-}$*) pairs. Mice entered protocols at 8 weeks of age and were analyzed between 22 and 26 weeks of age according to protocols. When not in HFD or GTT/ITT protocols, mice were weighed at 8 weeks and sacrificed at 22 weeks (5 months) of age. At sacrifice, organs (liver, gonadal and renal fat masses) were removed and weighed and then flash-frozen or fixed in 4% formaldehyde for further analyzes. All mice were kept within the animal facilities and according to the policies of the Laboratoire d'Exploration Fonctionnelle de Luminy (Marseilles, France). WT mice used in Fig 3A, D and E and Supplementary Fig S2C were C57BL/6J (i.e. C57BL/6 from Jackson Laboratory).

## HFD protocol

Male mice (8 week old) were used since (i) weight gain upon aging of TP53INP1 KO compared to WT males is more pronounced than females, and (ii) males gain more weight than females when fed with HFD (Hwang *et al*, 2010). Mice were randomly assigned to three cohorts (HFD protocol, HFD protocol with NAC, HFD protocol followed by GTT and ITT) containing four groups each (TP53INP1 WT CTRL and HFD and TP53INP1 KO CTRL and HFD). Mice were housed (two mice per cage) under a 12-h light and 12-h dark cycle. They were fed with either standard chow (CTRL: Special Diet Services #824050; 20% protein, 10% fat, 70% carbohydrates) or high-fat diet (HFD: Special Diet Services #824054; 20% protein, 60% fat, 20% carbohydrates) with *ad libitum* access to food. During 16 weeks (or 18 weeks for GTT/ITT cohort), weekly food intake was measured by monitoring the weight of the remaining food at cage changing, always at the same daytime moment. Concurrently, mice were weighed. One cohort was given antioxidant NAC (Sigma-Aldrich, Saint-Quentin Fallavier, France) at 10 mg/ml (1%) in drinking water during all protocol. Except for GTT/ITT cohort, glycemia was taken at beginning and end of the protocol using a hand-held glucometer (One-Touch® Ultra®; Lifescan, Issy les Moulineaux, France) from blood sampled from the tail vein of 6-h-fasted mice. At week 16, mice were sacrificed by cervical dislocation, and organs were weighed and stored.

## Glucose tolerance and insulin tolerance tests (GTT and ITT)

For the GTT/ITT cohort, GTT test was performed at week 16 of HFD protocol, ITT at week 17, and sacrifice at week 18. Glucose (1 g/kg body weight, GTT) or insulin (0.70 U/kg body weight, NovoRapid®, Novo Nordisk®, Chartres, France, ITT) was injected intraperitoneally to 6-h-fasted mice. Glycemia was taken from tail vein blood sample before and after injection at different time points during 120 (GTT) or 150 (ITT) min. Area under curve (AUC; GTT) and area above curve (AAC; ITT) were determined using Excel and the trapezoidal rule.

## Plasma insulin level measurement

Plasma insulin levels were determined using a sensitive rat insulin RIA kits according to manufacturer instructions (Millipore, Molsheim, France).

## NADP(H), [Ca$^{2+}$]$_c$ and insulin secretion

Islets were isolated after collagenase digestion of the pancreas from 3-month-old TP53INP1 WT and KO male mice and were used after an overnight culture in RPMI-1640 (Life Technologies, Cergy Pontoise, France) supplemented with 10 mM glucose and 10% fetal bovine serum (FBS). The medium used for the experiments was a Bicarbonate KRB supplemented with 3 mM glucose. For [Ca$^{2+}$]$_c$, NADP(H) and insulin secretion, the experiments were performed on 17 (WT) and 21 (KO) islets as previously reported (Ravier *et al*, 2014).

## Histological analysis

### Liver
Formaldehyde-fixed paraffin-embedded liver sections from HFD protocol mice were deparaffinized and stained with hematoxylin/eosin. Integrality of mounted stained sections surfaces was viewed on a Nikon microscope, and representative pictures were shown.

### Pancreas
Pancreases from 3-month-old TP53INP1 WT (*n* = 4) and KO (*n* = 4) male mice were spread into flat embedding cassettes, fixed with 4% paraformaldehyde, paraffin embedded and longitudinally sectioned through the pancreatic head-to-tail axis (4 μm thickness). Three pancreatic sections per mouse, separated by at least 100 μm, were stained with hematoxylin/eosin and scanned using a NanoZoomer slide scanner (Hamamatsu Photonics, Hamamatsu City, Japan). The islet numbers were quantified, and the area of each islet was measured with the NDP.view software, version 1.2.

## Cell culture

Cell lines were cultured in DMEM Glutamax medium (Life Technologies) supplemented with 10% (FBS) in a humidified atmosphere with 5% CO$_2$ at 37°C. TP53INP1 WT and TP53INP1 KO primary MEFs were obtained from embryos derived from homozygous breeding at 14.5 days postcoitum (E14.5) according to standard procedure. Immortalized MEFs (MEFi) were prepared from primary MEFs by sequential passages as for 3T3 cell line establishment. MEFs were cultured in the presence of penicillin (100 mU/ml) and streptomycin (100 mg/ml). They were used at early passages. HEK293T and U2OS cell lines were purchased from the American Type Culture Collection (Manassas, VA, USA). TP53INP1α-inducible U2OS cells (U2OSi), obtained by stable cotransfection with pVgRXR and pIND-TP53INP1α-EGFP vectors as previously reported (Gironella *et al*, 2007), were cultured in the presence of zeocin (0.05 mg/ml) and G418 (0.2 mg/ml).

## Cell treatments

Cells were plated in medium supplemented or not with 10 mM NAC and either treated 48 h later (80% confluency) with 1 mM hydrogen peroxide (H$_2$O$_2$) (Sigma-Aldrich) directly added in culture media or left untreated. After 1 h, cells were thoroughly rinsed twice with PBS and incubated 4 h with new culture medium containing or not 5 mM 3-MA (Early autophagic blocker, Sigma-Aldrich), 10 mM NAC, 10 μM GW9662 (Irreversible PPARγ antagonist; Sigma-Aldrich)

and 50 μM PNU-74654 (Wnt/β-catenin pathway inhibitor; Sigma-Aldrich).

## Induction and transfection

In TP53INP1α-inducible U2OS cells, TP53INP1α-GFP expression was induced on 70% confluent cells using 10 μM ponasterone A (Life Technologies) for 24 h. DNA transfections were performed using FuGENE HD (Promega) according to the manufacturer's instructions on 75% confluent cells 24 h before experiment.

## Flow cytometry

MEFi were incubated during 10 min at 37°C with 5 μM MitoSOX™ Red (Life Technologies #M36008) or 200 nM MitoTracker® Deep Red (Life Technologies #M22426) diluted in HBSS (Hank's buffered salt solution; Life Technologies). Cells were trypsinized and rinsed by centrifugation (1,200 g, 5 min) with PBS. They were then analyzed on a FACSCalibur flow cytometer (BD Biosciences, Le Pont de Claix, France). Data analysis was performed using FlowJO (Tree-star, Olten, Switzerland) software.

## Transmission electron microscopy (TEM)

MEFi were seeded in 10-cm dishes (7.5 × 10^6 cells) 48 h before treatment. Cells were then rinsed twice with PBS and fixed for 1 h in cacodylate sodium buffer 0.2 M, pH 7.2, containing 2.5% glutar-aldehyde, 8% paraformaldehyde and 0.01% CaCl₂. Samples were then treated as described previously (Baron Gaillard *et al*, 2011). Observations were performed on an EM 912 electron microscope (Zeiss) at 100-kV acceleration equipped with a BioScan camera (Model 792; Gatan, Warrendale, PA, USA). Images were acquired with the Digital Micrograph software (Gatan). Quantification of the number of mitochondria, mitophagic vacuoles and lipid droplets normalized by cytoplasmic surface area was done by counting these structures on 40 images for which surface occupied by cell cytoplasm has been determined. Quantification of mean size of mito-chondria was done by using area of an ellipse formula (area = longer diameter × smaller diameter × π), longer diameter of mitochondria being determined on images and smaller diameter considered as half of longer diameter.

## High-resolution respirometry

High-resolution respirometry was performed using a 2-ml chamber OROBOROS® Oxygraph 2K (Oroboros Instruments, Innsbruck, Austria) at 37°C. Respiration rates were calculated as the time deriv-ative of oxygen concentration measured in the closed respirometer and expressed per million viable cells and corrected by non-mitochondrial oxygen consumption (antimycin A). The amplified signal was recorded in a computer with online display of the calibrated oxygen concentration and oxygen flux (DatLab software for data acquisition and analysis; Oroboros Instruments). Intact cells (0.5 × 10^6 cells/ml) were analyzed in their respective bioener-getic substrate-containing cultivation medium. ROUTINE respiration (no additions), LEAK respiration (oligomycin-inhibited, 8 μg/ml) and ETS capacity (maximum non-coupled respiration induced by stepwise (typically 2–3 steps) titration of carbonyl cyanide

*p*-(trifluoromethoxy) phenylhydrazone (FCCP), 0.8 mM dissolved in ethanol) were determined. Oxygen consumption was also measured on cells permeabilized with digitonin (8 μg/ml) in respiration buffer (10 mM KH₂PO₄, 300 mM mannitol, 10 mM KCl, 5 mM MgCl₂, 1 mM EGTA and 1 mg/ml BSA fatty acid free) at final cell densities 0.5 × 10^6 cells per milliliter. Respiration state 3 and 4 (LEAK) and ETS capacity were measured with pyruvate, malate and succinate (5, 5 and 10 mM, respectively) or palmitoylcarnitine and malate (40 μM and 5 mM, respectively). Activity of complex IV (cytochrome c oxidase) was determined by oxygraphy with trimethyl pentanediol (TMPD) as substrate.

## Fluorescence microscopy

### Bodipy staining
Since Bodipy fluoresces in green, we used expression vectors encod-ing TP53INP1 isoforms tagged in red fluorescence. U2OSi cells were cotransfected by TP53INP1α + β-DsRed-N1 vector (containing human full-length TP53INP1 cDNAs) or empty pcDNA4/V5-His vector (Clontech, Saint-Germain-en-Laye, France) 24 h prior experi-ment. Cells (MEFi or U2OS) plated on glass coverslips in 12-well plates were treated as indicated and then fixed with 4% paraformal-dehyde. Cells were washed with PBS and stained with BODIPY® 493–503 7.5 μg/ml (Life Technologies #D3922) in PBS during 5 min. Slides were then mounted in ProLong Gold antifade reagent with DAPI (Invitrogen) for imaging. Fluorescent images were captured using a Nikon microscope Eclipse 90I.

### Mitotracker-LC3 co-staining
MEFi cells were plated on glass coverslips in 12-well plates 48 h prior experiment. Cells were incubated in a humidified atmo-sphere with 5% CO₂ at 37°C during 15 min with MitoTracker® Red CMXRos 100 nM (Life Technologies #M-7512) diluted in warmed culture medium. After 2 washes with 1× PBS, cells were fixed during 15 min at 37°C with warmed 4% paraformaldehyde. Following fixation, cells were incubated in blocking buffer (3% BSA, 0.01% saponin in 1× PBS) containing 0.2 M glycine and 10% goat serum for 30 min. Then, cells were incubated 1 h at room temperature with primary antibody anti-LC3 (PM036-1:500; MBL, Nanterre, France) diluted in blocking buffer and washed three times before the addition of secondary antibody (Alexa Fluor 488 goat anti-rabbit, A-11034-1:500; Invitrogen). After 1 h of incubation at room temperature, cells were washed three times and slides were mounted in ProLong Gold antifade reagent with DAPI (Invitrogen) for imaging. Fluorescent images were captured using a Zeiss LSM 510 confocal microscope (Carl Zeiss, Le Pecq, France). Quantification of Mitotracker-LC3-positive puncta (= mitophagic figures) was done in 10 cells per genotype in three independent experiments.

### Insulin/TP53INP1 co-staining
Insulin and TP53INP1 immunoreactivity were revealed with an anti-insulin antibody (1:200, DakoCytomation, Ely, UK) and with E12 mAb specific of TP53INP1 (1:100) (Gironella *et al*, 2007), respec-tively. Images were captured from mouse pancreatic sections and single human islet beta cell using a Zeiss Nipkov spinning disk confocal microscope (Hodson *et al*, 2013). Base images were captured and exported as TIFF files; figures were created using

Adobe Photoshop 11. No manipulations other than global contrast and brightness adjustments were performed on images.

## Denaturing lysis

Cells were resuspended in denaturing lysis buffer (8 M urea, 0.1 M $Na_2HPO_4/NaH_2PO_4$, 0.01 M Tris–HCl, pH 8.0, 0.5% Triton X-100). Then, proteins were resolved by SDS–PAGE and immunoblotted.

## Mitochondria isolation

### From cells

TP53INP1α-inducible U2OS cells were seeded in 15-cm dishes ($7.5 \times 10^6$ cells) 48 h before being collected by scrapping. Mitochondria were isolated according to the manufacturer's instructions of Mitochondria Isolation Kit for Cultured Cells (Abcam #ab110171, Paris, France). Briefly, after one freeze–thaw cycle, pellets from 2 dishes were resuspended in 750 µl Reagent A at 5.0 mg/ml protein and incubated on ice for 10 min. Cells were then disrupted with a Dounce homogenizer. After centrifugation (1,000 *g*, 10 min, 4°C), supernatants (SN1) were saved. Pellets were resuspended in 750 µl Reagent B, ruptured with Dounce homogenizer and centrifugated again. Supernatants (SN2) were collected and added to SN1. Few microliters of SN1 + SN2 was kept as total protein cell lysates. After spinning of remaining SN1 + SN2 (12,000 *g*, 10 min, 4°C), supernatants were discarded: pellets were resuspended in 450 µl Reagent C containing protease inhibitors cocktail (Sigma-Aldrich), forming mitochondrial lysates.

### From tissue

Six TP53INP1 WT and six KO male mice (3 month old) were sacrificed and their livers sampled. Mitochondrial lysates were extracted from 300 mg of fresh liver according to the manufacturer's instructions of Mitochondria Isolation Kit for Tissue (Abcam #ab110169). A small volume of lysates before first high-speed centrifugation (12,000 *g*) was kept as total protein lysates.

## Coprecipitation assay

HEK293T cells in six-well plates were cotransfected by TP53INP1α- or β-NTAP vector (containing human full-length TP53INP1 cDNAs) or empty pNTAP vector (Agilent, Massy, France). After 24 h of transfection, cells were harvested by scraping and lysed and protein complexes were purified using streptavidin-containing resin according to the manufacturer's instructions of InterPlay Mammalian TAP Purification Kit (Agilent). Then, proteins were resolved by SDS–PAGE and immunoblotted.

## Immunoblotting

After boiling in Laemmli buffer (20 mM Tris pH 6.8, 2 M β-mercaptoethanol, SDS 9%, glycerol 30%), proteins from total lysates, mitochondrial lysates or co-immunoprecipitations were resolved by SDS–PAGE, transferred to polyvinylidene fluoride membrane, blocked in 5% non-fat milk in phosphate-buffered saline (PBS)/Tween-20, blotted and developed with antibodies specific for ATGL (2439-1:1,000; Cell Signaling Technology, Saint-Quentin-en-Yvelines, France), BNIP3 (ab10433-1:250; Abcam), BNIP3L/NIX (ab8399-1:1,000; Abcam), CPT1A (ab128568-1:800; Abcam), CPT1B (ab104662-1:800; Abcam), MGLL (ab119777-1:1,000; Abcam), PARKIN (ab15954-1:1,050; Abcam), PGC-1α (sc13067-1:200; Santa Cruz Biotechnology, Heidelberg, Germany), PINK1 (BC100-494-1:500; Novus Biologicals, Montluçon, France), PPARγ (sc72-73-1:1,250; Santa Cruz Biotechnology), TP53INP1 [rat monoclonal antibody generated in our laboratory, clone F8 (Saadi *et al*, 2013), 2 µg/ml], VDAC1 (ab14734-1:2,500; Abcam), β-catenin (sc1496-1:500; Santa Cruz Biotechnology) or β-tubulin (T4026-1:4,000; Sigma-Aldrich). Secondary antibodies were purchased from Santa Cruz Biotechnology: anti-rabbit horseradish peroxidase (HRP) conjugate (sc-2004-1:4,000) and anti-mouse HRP conjugate (sc-2005-1:6,000). Immunoblots were developed using the Immobilon Western Chemiluminescent HRP Substrate (Millipore). Chemiluminescence was detected using Fusion FX7 device (Fisher Bioblock Scientific, Illkirch, France). The experiments for the immunoblotting were performed at least three times with comparable results.

## Real-time quantitative PCR

Total RNAs from islets and exocrine pancreas (from mouse and rat) were extracted and DNase-treated using the RNeasy microkit from Qiagen, according to the manufacturer's instructions. Total RNAs from other tissues (spleen, liver) and β-cell lines were extracted using RNAnow (Ozyme) and treated with DNase (Ambion) according to the manufacturers' instructions. For HFD islets, C57BL/6J female mice purchased from Charles River (France) were fed either with a standard normal diet (ND, 5 kcal % fat) or a HFD containing lard (45 kcal % fat; D12451; Research Diets, New Brunswick, NJ, USA) from 8 weeks for 23 weeks. Islets were isolated after collagenase digestion of the pancreas (Broca *et al*, 2009). The quality of the islet preparations was validated by measuring the expression of *Insulin* and *Elastase 3b* by RT–qPCR in both exocrine and islet RNAs. The presence of exocrine tissue in the islets was < 5% (mean 1.7%, not shown). INS-1E and MIN6 cells were grown and maintained as described previously (Broca *et al*, 2009; Quoyer *et al*, 2010).

Reverse transcription was performed on total RNA using random hexamer oligonucleotides and MoMuLV-RT (Invitrogen). Real-time PCR amplification was performed in duplicate, using the 7500 System (Applied Biosystems) and according to the manufacturer's instructions. The sequences of the primers used were as follows: *Trp53inp1*: GTTGACTTCATAGATACCTGCCC/GTGTGCTCTGCT-GAGGACTC which were validated both on rat and mouse cDNAs; *Tubb2*: CAAGGCTTTCCTGCACTGGT/AACTCCATCTCGTCCATGCC, which were validated both on rat and mouse cDNAs; *mHprt*: GCAG-TACAGCCCCAAAATGG/GGTCCTTTTCACCAGCAAGCT; and *rHprt*: CAAAATGGTTAAGGTTGCAAGCT/AACACTTCGAGAGGTCCTTTT-CAC. The level of expression of each gene X was normalized to the geometric mean of the expression levels of two housekeeping genes (*Hprt* and *Tubb2*) according to the formula: X/geometric mean $(Hprt, Tubb2) = 2^{-(Ct(X) - \text{arithmetic mean } (Ct(Hprt), Ct(Tubb2)))}$, where *C*t is the threshold cycle.

## Statistical analysis

Results are expressed as the mean ± SEM of results from at least two independent experiments. Statistical analyses were mainly

performed via Student's *t*-tests except Mann–Whitney *U*-tests for Fig 6. $P < 0.05$ was considered as significant.

## Human studies

Morbidly obese patients ($n = 39$) were recruited through the Department of Digestive Surgery and Liver Transplantation (Nice Hospital) where they underwent bariatric surgery for their morbid obesity. Bariatric surgery was indicated for these patients in accordance with French guidelines. Exclusion criteria were presence of a hepatitis B or hepatitis C infection, excessive alcohol consumption (> 20 g/day) or another cause of chronic liver disease as previously described (Anty *et al*, 2006; Bekri *et al*, 2006; Bertola *et al*, 2009). The characteristics of the study groups are described in Supplementary Table S2. Before surgery, fasting blood samples were obtained and used to measure alanine amino transferase (ALT), glucose, insulin, HDL cholesterol, LDL cholesterol and triglycerides. Insulin resistance was calculated using the homeostatic model assessment (HOMA-IR) index (Wallace *et al*, 2004). Surgical liver biopsies were obtained during surgery, and no ischemic preconditioning had been performed. Histopathological analysis was performed to evaluate hepatic steatosis (0, < 5%; 1, 5–30%; 2, > 30–60%; 3, > 60%).

Total liver RNA was extracted from human tissues using the RNeasy Mini Kit (Qiagen, Contraboeuf, France) and treated with Turbo DNA free (Applied Biosystems, Contraboeuf, France) following the manufacturer's protocol. The quantity and quality of the RNA were determined using the Agilent 2100 Bioanalyser with RNA 6000 Nano Kit (Agilent Technologies). Total RNA (1 μg) was reverse-transcribed with a High-Capacity cDNA Reverse Transcription Kit (Applied Biosystems). Real-time quantitative PCR was performed in duplicate for each sample using the ABI Step One Fast Real-Time PCR System (Applied Biosystems) as previously described (Kleiner *et al*, 2005). TaqMan gene expression assays were purchased from Applied Biosystems: RPLP0 (Hs99999902_m1) and TP53INP1 (Hs01003820_m1). Gene expression was normalized to the housekeeping gene human *RPLP0* (ribosomal phosphoprotein large P0) calculated based on the comparative cycle threshold *C*t method ($2^{-\Delta\Delta Ct}$). Results are expressed as the mean ± SEM. Statistical significance of differential human gene expression between two study groups was determined using the non-parametric Mann–Whitney *U*-test with the Δ*C*t of each group. Correlations were analyzed using the Spearman's rank correlation test. $P < 0.05$ was considered as significant.

## Study approval

Care and manipulation of mice were performed in accordance with national and European legislation on animal experimentation and were approved by the Aix-Marseille University Institutional Animal Care and Use Committee. Regarding human study, all subjects gave their informed written consent to participate in this study in accordance with French legislation regarding Ethics and Human Research (Huriet-Serusclat law). The 'Comité Consultatif de Protection des Personnes dans la Recherche Biomédicale de Nice' approved the study (07/04:2003, No 03.017).

**Supplementary information** for this article is available online: http://embomolmed.embopress.org

## The paper explained

### Problem

The gene encoding tumor protein 53-induced nuclear protein 1 (TP53INP1) is a target of the tumor suppressor p53 and displays itself a tumor suppressor activity. TP53INP1 contributes to maintain cellular homeostasis in response to stress, in synergy with p53. Interestingly, the tumor suppressor activity of TP53INP1 is associated with its anti-oxidant function, shedding light in the link between the oxidative stress response and carcinogenesis. In addition, (i) TP53INP1 is involved in autophagy, a crucial catabolism process for cell homeostasis, and (ii) a genome-wide association study (GWAS) published in 2010 identified *TP53INP1* as a new type 2 diabetes susceptibility locus, but a pathological mechanism was not identified. In this context, this study further investigates the importance of TP53INP1 in cell metabolism regulation, associated with its implication in autophagy and redox homeostasis.

### Results

In this paper, we demonstrate that *TP53INP1* is involved in the prevention of redox-driven obesity, which promotes insulin resistance, and thus type 2 diabetes. Furthermore, we unveil the impact of TP53INP1 on mitochondrial homeostasis, both quantitatively and qualitatively, as well as the central role of mitophagy alterations in chronic oxidative stress observed in the absence of TP53INP1. Thus, we provide a mechanism of TP53INP1 function in redox-dependent metabolism homeostasis.

### Impact

TP53INP1 is a novel molecular actor in obesity and type 2 diabetes, thus being a promising target in prevention or therapy of metabolic syndrome. Thus, this study provides a useful preclinical model of mice prone to metabolic alterations.

## Author contributions

MS conceived the project, designed and performed most of the experiments (HFD protocol, NAC treatment, dissection of mice, GTT and ITT, flow cytometry, TEM, cell treatments, mitochondria isolation, coprecipitations, WB, Bodipy staining), analyzed the data and prepared the original draft of the manuscript. LPo and PN'G obtained preliminary results at the origin of the study. MN provided experimental and technical support for flow cytometry and analyzed data. MN and FC provided experimental and technical support for mice analysis. FG provided experimental advice for metabolism analysis. LPe, J-FD and SS performed oxygraphy experiments and analyzed data. AV performed qPCR experiments on rat and mouse cells/tissues and analyzed data. GB and MAR performed plasma insulin, NADP(H) and $[Ca^{2+}]_c$ level measurements and HFD (45% fat)-fed C57Bl/6 mice experiments and analyzed data. SB, AT and PG performed experiments on obese patients' liver samples and analyzed data. GM and GAR performed immunofluorescence analysis on mouse pancreatic sections and single human islet cells supplied by PM. DM performed measure of mass on murine pancreatic islets. AC conceived and supervised the project, and wrote the paper. All authors discussed the results and commented on the manuscript.

## Conflict of interest

The authors declare that they have no conflict of interest.

# References

Anty R, Bekri S, Luciani N, Saint-Paul MC, Dahman M, Iannelli A, Amor IB, Staccini-Myx A, Huet PM, Gugenheim J *et al* (2006) The inflammatory C-reactive protein is increased in both liver and adipose tissue in severely obese patients independently from metabolic syndrome, Type 2 diabetes, and NASH. *Am J Gastroenterol* 101: 1824−1833

Baron Gaillard CL, Pallesi-Pocachard E, Massey-Harroche D, Richard F, Arsanto JP, Chauvin JP, Lecine P, Kramer H, Borg JP, Le Bivic A (2011) Hook2 is involved in the morphogenesis of the primary cilium. *Mol Biol Cell* 22: 4549−4562

Bekri S, Gual P, Anty R, Luciani N, Dahman M, Ramesh B, Iannelli A, Staccini-Myx A, Casanova D, Ben Amor I *et al* (2006) Increased adipose tissue expression of hepcidin in severe obesity is independent from diabetes and NASH. *Gastroenterology* 131: 788−796

Bertola A, Deveaux V, Bonnafous S, Rousseau D, Anty R, Wakkach A, Dahman M, Tordjman J, Clement K, McQuaid SE *et al* (2009) Elevated expression of osteopontin may be related to adipose tissue macrophage accumulation and liver steatosis in morbid obesity. *Diabetes* 58: 125−133

Bondia-Pons I, Ryan L, Martinez JA (2012) Oxidative stress and inflammation interactions in human obesity. *J Physiol Biochem* 68: 701−711

Broca C, Quoyer J, Costes S, Linck N, Varrault A, Deffayet PM, Bockaert J, Dalle S, Bertrand G (2009) beta-Arrestin 1 is required for PAC1 receptor-mediated potentiation of long-lasting ERK1/2 activation by glucose in pancreatic beta-cells. *J Biol Chem* 284: 4332−4342

Calder PC, Ahluwalia N, Brouns F, Buetler T, Clement K, Cunningham K, Esposito K, Jonsson LS, Kolb H, Lansink M *et al* (2011) Dietary factors and low-grade inflammation in relation to overweight and obesity. *Br J Nutr* 106(Suppl 3): S5−S78

Cano CE, Gommeaux J, Pietri S, Culcasi M, Garcia S, Seux M, Barelier S, Vasseur S, Spoto RP, Pebusque MJ *et al* (2009) Tumor protein 53-induced nuclear protein 1 is a major mediator of p53 antioxidant function. *Cancer Res* 69: 219−226

Cauchi S, Ezzidi I, El Achhab Y, Mtiraoui N, Chaieb L, Salah D, Nejjari C, Labrune Y, Yengo L, Beury D *et al* (2012) European genetic variants associated with type 2 diabetes in North African Arabs. *Diabetes Metab* 38: 316−323

Chawla A, Nguyen KD, Goh YP (2011) Macrophage-mediated inflammation in metabolic disease. *Nat Rev Immunol* 11: 738−749

Crujeiras AB, Diaz-Lagares A, Carreira MC, Amil M, Casanueva FF (2013) Oxidative stress associated to dysfunctional adipose tissue: a potential link between obesity, type 2 diabetes mellitus and breast cancer. *Free Radic Res* 47: 243−256

Deng T, Lyon CJ, Minze LJ, Lin J, Zou J, Liu JZ, Ren Y, Yin Z, Hamilton DJ, Reardon PR *et al* (2013) Class II major histocompatibility complex plays an essential role in obesity-induced adipose inflammation. *Cell Metab* 17: 411−422

Eizirik DL, Sammeth M, Bouckenooghe T, Bottu G, Sisino G, Igoillo-Esteve M, Ortis F, Santin I, Colli ML, Barthson J *et al* (2012) The human pancreatic islet transcriptome: expression of candidate genes for type 1 diabetes and the impact of pro-inflammatory cytokines. *PLoS Genet* 8: e1002552

Forte V, Pandey A, Abdelmessih R, Forte G, Whaley-Connell A, Sowers JR, McFarlane SI (2012) Obesity, Diabetes, the Cardiorenal Syndrome, and Risk for Cancer. *Cardiorenal Med* 2: 143−162

Gironella M, Seux M, Xie MJ, Cano C, Tomasini R, Gommeaux J, Garcia S, Nowak J, Yeung ML, Jeang KT *et al* (2007) Tumor protein 53-induced nuclear protein 1 expression is repressed by miR-155, and its restoration inhibits pancreatic tumor development. *Proc Natl Acad Sci USA* 104: 16170−16175

Gommeaux J, Cano C, Garcia S, Gironella M, Pietri S, Culcasi M, Pebusque MJ, Malissen B, Dusetti N, Iovanna J *et al* (2007) Colitis and colitis-associated cancer are exacerbated in mice deficient for tumor protein 53-induced nuclear protein 1. *Mol Cell Biol* 27: 2215−2228

Gregor MF, Hotamisligil GS (2011) Inflammatory mechanisms in obesity. *Annu Rev Immunol* 29: 415−445

Greiner T, Backhed F (2011) Effects of the gut microbiota on obesity and glucose homeostasis. *Trends Endocrinol Metab* 22: 117−123

Gupta SC, Hevia D, Patchva S, Park B, Koh W, Aggarwal BB (2012) Upsides and downsides of reactive oxygen species for cancer: the roles of reactive oxygen species in tumorigenesis, prevention, and therapy. *Antioxid Redox Signal* 16: 1295−1322

Hodson DJ, Mitchell RK, Bellomo EA, Sun G, Vinet L, Meda P, Li D, Li WH, Bugliani M, Marchetti P *et al* (2013) Lipotoxicity disrupts incretin-regulated human beta cell connectivity. *J Clin Invest* 123: 4182−4194

Hwang LL, Wang CH, Li TL, Chang SD, Lin LC, Chen CP, Chen CT, Liang KC, Ho IK, Yang WS *et al* (2010) Sex differences in high-fat diet-induced obesity, metabolic alterations and learning, and synaptic plasticity deficits in mice. *Obesity (Silver Spring)* 18: 463−469

Jiang PH, Motoo Y, Iovanna JL, Pebusque MJ, Xie MJ, Okada G, Sawabu N (2004) Tumor protein p53-induced nuclear protein 1 (TP53INP1) in spontaneous chronic pancreatitis in the WBN/Kob rat: drug effects on its expression in the pancreas. *J Pancreas* 5: 205−216

Kameswaran V, Bramswig NC, McKenna LB, Penn M, Schug J, Hand NJ, Chen Y, Choi I, Vourekas A, Won KJ *et al* (2014) Epigenetic regulation of the DLK1-MEG3 microRNA cluster in human type 2 diabetic islets. *Cell Metab* 19: 135−145

Khoo NK, Cantu-Medellin N, Devlin JE, St Croix CM, Watkins SC, Fleming AM, Champion HC, Mason RP, Freeman BA, Kelley EE (2012) Obesity-induced tissue free radical generation: an in vivo immuno-spin trapping study. *Free Radic Biol Med* 52: 2312−2319

Kleiner DE, Brunt EM, Van Natta M, Behling C, Contos MJ, Cummings OW, Ferrell LD, Liu YC, Torbenson MS, Unalp-Arida A *et al* (2005) Design and

validation of a histological scoring system for nonalcoholic fatty liver disease. *Hepatology* 41: 1313–1321

van Kruijsdijk RC, van der Wall E, Visseren FL (2009) Obesity and cancer: the role of dysfunctional adipose tissue. *Cancer Epidemiol Biomarkers Prev* 18: 2569–2578

Lavallard VJ, Meijer AJ, Codogno P, Gual P (2012) Autophagy, signaling and obesity. *Pharmacol Res* 66: 513–525

Leboucher A, Laurent C, Fernandez-Gomez FJ, Burnouf S, Troquier L, Eddarkaoui S, Demeyer D, Caillierez R, Zommer N, Vallez E *et al* (2013) Detrimental effects of diet-induced obesity on tau pathology are independent of insulin resistance in tau transgenic mice. *Diabetes* 62: 1681–1688

Liang Y, Liu J, Feng Z (2013) The regulation of cellular metabolism by tumor suppressor p53. *Cell Biosci* 3: 9

Maddocks OD, Vousden KH (2011) Metabolic regulation by p53. *J Mol Med (Berl)* 89: 237–245

Mauvezin C, Orpinell M, Francis VA, Mansilla F, Duran J, Ribas V, Palacin M, Boya P, Teleman AA, Zorzano A (2010) The nuclear cofactor DOR regulates autophagy in mammalian and Drosophila cells. *EMBO Rep* 11: 37–44

Moldes M, Zuo Y, Morrison RF, Silva D, Park BH, Liu J, Farmer SR (2003) Peroxisome-proliferator-activated receptor gamma suppresses Wnt/beta-catenin signalling during adipogenesis. *Biochem J* 376: 607–613

Murphy MP (2009) How mitochondria produce reactive oxygen species. *Biochem J* 417: 1–13

Musso G, Gambino R, Cassader M (2010) Obesity, diabetes, and gut microbiota: the hygiene hypothesis expanded? *Diabetes Care* 33: 2277–2284

N'Guessan P, Pouyet L, Gosset G, Hamlaoui S, Seillier M, Cano CE, Seux M, Stocker P, Culcasi M, Iovanna JL *et al* (2011) Absence of tumor suppressor tumor protein 53-induced nuclear protein 1 (TP53INP1) sensitizes mouse thymocytes and embryonic fibroblasts to redox-driven apoptosis. *Antioxid Redox Signal* 15: 1639–1653

Novak I (2012) Mitophagy: a complex mechanism of mitochondrial removal. *Antioxid Redox Signal* 17: 794–802

Nowak J, Archange C, Tardivel-Lacombe J, Pontarotti P, Pebusque MJ, Vaccaro MI, Velasco G, Dagorn JC, Iovanna JL (2009) The TP53INP2 protein is required for autophagy in mammalian cells. *Mol Biol Cell* 20: 870–881

Pothiwala P, Jain SK, Yaturu S (2009) Metabolic syndrome and cancer. *Metab Syndr Relat Disord* 7: 279–288

Pouyet L, Carrier A (2010) Mutant mouse models of oxidative stress. *Transgenic Res* 19: 155–164

Quoyer J, Longuet C, Broca C, Linck N, Costes S, Varin E, Bockaert J, Bertrand G, Dalle S (2010) GLP-1 mediates antiapoptotic effect by phosphorylating Bad through a beta-arrestin 1-mediated ERK1/2 activation in pancreatic beta-cells. *J Biol Chem* 285: 1989–2002

Ravier MA, Leduc M, Richard J, Linck N, Varrault A, Pirot N, Roussel MM, Bockaert J, Dalle S, Bertrand G (2014) beta-Arrestin2 plays a key role in the modulation of the pancreatic beta cell mass in mice. *Diabetologia* 57: 532–541

Rolo AP, Teodoro JS, Palmeira CM (2012) Role of oxidative stress in the pathogenesis of nonalcoholic steatohepatitis. *Free Radic Biol Med* 52: 59–69

Rufini A, Niklison-Chirou MV, Inoue S, Tomasini R, Harris IS, Marino A, Federici M, Dinsdale D, Knight RA, Melino G *et al* (2012) TAp73 depletion accelerates aging through metabolic dysregulation. *Genes Dev* 26: 2009–2014

Saadi H, Seillier M, Sandi MJ, Peuget S, Kellenberger C, Gravis G, Dusetti NJ, Iovanna JL, Rocchi P, Amri M *et al* (2013) Development of an ELISA detecting Tumor Protein 53-Induced Nuclear Protein 1 in serum of prostate cancer patients. *Results Immunol* 3: 51–56

Sahini N, Borlak J (2014) Recent insights into the molecular pathophysiology of lipid droplet formation in hepatocytes. *Prog Lipid Res* 54: 86–112

Sala D, Ivanova S, Plana N, Ribas V, Duran J, Bach D, Turkseven S, Laville M, Vidal H, Karczewska-Kupczewska M *et al* (2014) Autophagy-regulating TP53INP2 mediates muscle wasting and is repressed in diabetes. *J Clin Invest* 124: 1914–1927

Seillier M, Peuget S, Gayet O, Gauthier C, N'Guessan P, Monte M, Carrier A, Iovanna JL, Dusetti NJ (2012) TP53INP1, a tumor suppressor, interacts with LC3 and ATG8-family proteins through the LC3-interacting region (LIR) and promotes autophagy-dependent cell death. *Cell Death Differ* 19: 1525–1535

Seux M, Peuget S, Montero MP, Siret C, Rigot V, Clerc P, Gigoux V, Pellegrino E, Pouyet L, N'Guessan P *et al* (2011) TP53INP1 decreases pancreatic cancer cell migration by regulating SPARC expression. *Oncogene* 30: 3049–3061

Siegel AB, Zhu AX (2009) Metabolic syndrome and hepatocellular carcinoma: two growing epidemics with a potential link. *Cancer* 115: 5651–5661

Singh R, Cuervo AM (2011) Autophagy in the cellular energetic balance. *Cell Metab* 13: 495–504

Su X, Gi YJ, Chakravarti D, Chan IL, Zhang A, Xia X, Tsai KY, Flores ER (2012) TAp63 is a master transcriptional regulator of lipid and glucose metabolism. *Cell Metab* 16: 511–525

Tomasini R, Samir AA, Vaccaro MI, Pebusque MJ, Dagorn JC, Iovanna JL, Dusetti NJ (2001) Molecular and functional characterization of the stress-induced protein (SIP) gene and its two transcripts generated by alternative splicing. SIP induced by stress and promotes cell death. *J Biol Chem* 276: 44185–44192

Tomasini R, Samir AA, Carrier A, Isnardon D, Cecchinelli B, Soddu S, Malissen B, Dagorn JC, Iovanna JL, Dusetti NJ (2003) TP53INP1s and homeodomain-interacting protein kinase-2 (HIPK2) are partners in regulating p53 activity. *J Biol Chem* 278: 37722–37729

Tomasini R, Seux M, Nowak J, Bontemps C, Carrier A, Dagorn JC, Pebusque MJ, Iovanna JL, Dusetti NJ (2005) TP53INP1 is a novel p73 target gene that induces cell cycle arrest and cell death by modulating p73 transcriptional activity. *Oncogene* 24: 8093–8104

Voight BF, Scott LJ, Steinthorsdottir V, Morris AP, Dina C, Welch RP, Zeggini E, Huth C, Aulchenko YS, Thorleifsson G *et al* (2010) Twelve type 2 diabetes susceptibility loci identified through large-scale association analysis. *Nat Genet* 42: 579–589

Wallace TM, Levy JC, Matthews DR (2004) Use and abuse of HOMA modeling. *Diabetes Care* 27: 1487–1495

Zhang J, Ney PA (2009) Role of BNIP3 and NIX in cell death, autophagy, and mitophagy. *Cell Death Differ* 16: 939–946